Effect of Taper Waist Diameter on the Sensitivity of Multicore Fiber Coupler-Based Temperature and Strain Sensors

Valeria Hernández-Ambato, David Barrera, Elham Nazemosadat, Hugo Moreno, *Member, IEEE*, and Salvador Sales, *Senior Member, IEEE*

***Abstract*—This paper analyses the effect of the waist diameter on the sensitivity of different sensors based on non-adiabatic multicore fiber couplers. The sensors have been evaluated for high-temperature and strain measurements. A homogeneous 7-core multicore fiber has been used to fabricate three different coupler sensors based on the tapering technique, using a special CO_2 laser splicer. The waist length for all cases is 60 mm, while the studied waist diameters are 20 μm, 40 μm, and 60 μm. We report that the central core exhibits sensitivities of 62.1 pm/°C and −5.2 pm/$\mu\varepsilon$ for temperature and strain, respectively. The evaluated high-temperature range is from 100 °C to 600 °C, and the strain range is from 0 $\mu\varepsilon$ to 3333 $\mu\varepsilon$. Based on our findings regarding the evaluated waist diameters, we observed that the multicore fiber coupler with a waist diameter of 20 μm exhibits a large sensitivity to strain variations. Conversely, the sensor with a waist diameter of 60 μm demonstrates better sensitivity for temperature measurements. Additionally, we have used fan-in/fan-out optical devices to enable individual access to each core. This allowed us to extend our study and conduct sensitivity analysis in the outer cores.**

***Index Terms*—High-temperature, multicore fiber, strain, taper, waist diameter.**

I. Introduction

FIBER optic sensors are employed in various industrial applications thanks to their outstanding features, such as immunity to electromagnetic interference, low power consumption, resistance to corrosive environments, remote interrogation possibility, high thermal stability, and easy fabrication, which can be challenging for traditional sensors [1], [2]. They are widely used for measuring refractive index, temperature, liquid level, pressure, and strain, among others [2].

The aforementioned characteristics make fiber optic sensors ideal for harsh environments, where precision is crucial for ensuring safe and controlled processes. Examples of such applications include down-hole drilling for fossil fuels, power plant turbines, aerospace systems, and testing the structural health of different engineering structures, where the measurement of high temperatures and strain is necessary, even under extreme conditions [1], [3], [4]. Electronic sensors have frequently been used for temperature and strain measurements. However, they have some drawbacks, such as resistance errors, susceptibility to vibration, and high response time in electronic temperature sensors [5]. Moreover, conventional microelectromechanical systems (MEMS) and piezoelectric sensors cannot operate effectively at high temperatures [6]. Therefore, in critical scenarios, the inherent high thermal stability and the minimal risk of heat damage associated with fiber optic sensors make them the preferred choice over electronic sensors.

Temperature and strain monitoring have been typically carried out using fiber optic gratings. However, it has been reported in the literature that fiber grating sensors may degrade the optical performances of the resonant peaks when exposed to high-temperature environments [4]. Meanwhile, interferometers and couplers based on multicore fibers (MCFs) are promising cost-effective alternatives that also offer good thermal stability [1], [4]. A standard MCF has a well-spaced core pitch to ensure effective isolation between its cores. However, through some techniques, a propagating mode could be coupled between the cores. This property could be used to develop fiber optic sensors [7], [8], [9], [10], [11].

Antonio-Lopez et al. have proposed a temperature sensor that is fabricated via splicing a few-centimeter-long piece of MCF between two standard single mode fibers (SMFs) and reported a sensitivity of 52 pm/°C at high temperatures, between 100 °C and 1000 °C [1]. In the literature, other techniques, such as chemical etching [7] and tapering [4], [10], have been proposed to improve the performance of MCF-based temperature sensors. Meanwhile, several strain sensors fabricated in MCFs have also been reported, such as those based on Mach-Zehnder

Manuscript received 14 March 2024; revised 29 May 2024; accepted 12 July 2024. Date of publication 22 July 2024; date of current version 16 September 2024. This work was supported in part by MCIN/AEI/10.13039/501100011033 through I+D+i Projects under Grant SYNERGY PID2020-118310RB-I00 and Grant INSTILL PID2020-120071RJ-I00 and in part by Generalitat Valenciana under Grant PROMETEO 2021/015 Research Excellency Award, Grant IDIFEDER/2020/032, and Grant IDIFEDER/2021/050 GVA Infraestructura. The work of Valeria Hernández-Ambato was supported by Generalitat Valenciana under Grant GRISOLIAP/2020/083. An earlier conference version of this work was accepted in OFS-28, Hamamatsu, Japan, 2023 [DOI: 10.1364/OFS.2023.Tu3.87].*(Corresponding author: Valeria Hernández-Ambato.)*

Valeria Hernández-Ambato, David Barrera, and Salvador Sales are with the Photonics Research Labs, ITEAM, Universitat Politècnica de València, 46022 Valencia, Spain (e-mail: vheramb@upv.es; dabarvi@iteam.upv.es; ssales@dcom.upv.es).

Elham Nazemosadat is with the CalSens SL, Universitat Politècnica de València, 46022 Valencia, Spain (e-mail: elnazemos@cal-sens.com).

Hugo Moreno is with the Escuela Superior Politécnica de Chimborazo, Riobamba 060155, Ecuador (e-mail: h_moreno@espoch.edu.ec).

Color versions of one or more figures in this article are available at https://doi.org/10.1109/JLT.2024.3431712.

Digital Object Identifier 10.1109/JLT.2024.3431712

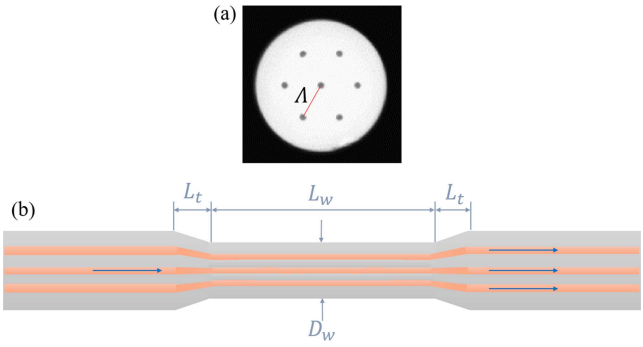

Fig. 1. (a) Cross-section image of the 7-core MCF. (b) Taper structure implemented in the MCF.

interferometers [10], [12], helical structure fiber [12] and mode-coupling theory [8], [13], [14], to mention a few. For instance, Gan et al. have presented a sensor based on a Mach-Zehnder interferometer integrating two MCF tapers with a waist diameter of around 42 μm, which could simultaneously measure temperature and strain, with maximum sensitivities of 53.20 pm/°C and -1.10 pm/$\mu\varepsilon$, respectively [10]. A shortcoming of fiber-based strain sensors is their inherent susceptibility to temperature [3], [10], [15]. Nevertheless, constructing a cross-sensitivity matrix could compensate for this relationship between the two parameters [3].

In sensors based on MCF couplers, it is well-known that the coupling among the cores and, consequently, the sensitivity of the sensor depends on the waist diameter of the tapered region. For instance, it has been demonstrated that in a refractive index sensor based on a tapered MCF, the smaller the waist diameter, the higher the sensitivity [13]. However, to our knowledge, how the waist diameter of an MCF coupler affects the sensitivity of temperature and strain measurements has not been investigated yet.

In this paper, we demonstrate temperature and strain sensors based on tapered MCFs. To study the impact of the taper waist diameter on the sensitivity of these sensors, we fabricated MCF couplers with different waist diameters. Moreover, we used fan-in/fan-out devices to exploit the spatial division multiplexing (SDM) technology typical in MCFs, to study the sensitivity in the outer cores besides the central core.

II. Analysis and Fabrication

The cross-section of the homogeneous MCF with seven cores used to fabricate the sensors is shown in Fig. 1(a). The cladding diameter is 125 μm, each core has a diameter of 6 μm, and the core pitch is $\Lambda = 35$ μm. It is a commercial optical fiber for communication systems. It should be noted that the measured crosstalk level in each core of the multicore fiber before tapering was less than -50 dB. This highlights the effective isolation between cores, a characteristic feature of this type of fiber.

The schematic structure of the proposed sensor is shown in Fig. 1(b). It is a non-adiabatic taper consisting of two transition zones, whose lengths are denoted as L_t. The sensor size is defined by the waist length, L_w, and the waist diameter, D_w, of the tapered region. Once a taper structure is fabricated in an MCF, coupling is introduced among the cores due to the reduction of the core diameter and pitch. The coupling coefficient could be defined using the coupled-mode theory, expressed as [16]

$$k = \frac{\lambda}{2\pi n_{co}} \frac{U^2}{r^2 V^2} \frac{K_0(W\Lambda/r)}{K_1^2(W)}, \tag{1}$$

where r is the core radius, λ is the operating wavelength, $K_m(x)$ are the modified Bessel functions of the second kind of order m $= [0, 1]$, $k_0 = 2\pi/\lambda$ is the wave number, n_{co} and n_{cl} are the core and cladding refractive indices, respectively, and β is the propagation constant of the fundamental mode of each core before coupling [16], [17]. The coupling coefficient also depends on the normalized frequency (V) and the normalized transverse propagation constants of the fundamental mode in the core (U) and cladding (W).

When light is launched into the central core, the normalized transmitted power in the central and outer cores at a propagation distance of z, denoted by A_c and A_o, respectively, can be derived according to the coupled-mode equations, as [16], [17]

$$|A_c(z)|^2 = \frac{1}{7} + \frac{6}{7}\cos^2\left(\sqrt{7}kz\right) \tag{2}$$

$$|A_o(z)|^2 = \frac{1}{7}\sin^2\left(\sqrt{7}kz\right) \tag{3}$$

It can be understood from (2) and (3), that the light injected in the central core oscillates periodically between the central and outer cores along the propagation distance. Moreover, the output power of each core depends on the coupling coefficient, which in turn is a function of the operating wavelength, as can be seen in (1). This means that for a fixed propagation distance, if the optical wavelength is continuously varied, the output power oscillates between the central and outer cores in a periodic manner. Thus, the power in each core is not just periodic in z, but also in λ.

Several multicore fiber tapers were fabricated using a CO_2 laser splicer (LZM100, Fujikura). The final diameter of each fabricated taper is shown in Fig. 2(a). All tapers have two transition lengths of $L_t = 5$ mm and a constant waist length of $L_w = 60$ mm. Three different waist diameters of $D_w = 20$ μm, 40 μm, and 60 μm were selected for our three sensors, corresponding to core pitch values of 5.6 μm, 11.2 μm, and 16.8 μm, respectively.

To measure the optical transmission spectrum of each sensor, we spliced the MCF end of the fan-in/fan-out devices (FAN-7C, Fibercore) to each end of the MCF taper to access the central and outer cores individually. An alternative method that allows individual core access is the offset splicing technique [17]. However, achieving simultaneous individual access to different cores is not possible in this scenario. The measured optical spectrum at the output of the central core, when light is launched into this core, is shown in Fig. 2(b). The separation between two consecutive dips represents the free spectral range (FSR). These values are 7.73 nm, 21.95 nm, and 29.52 nm for waist diameters of 20 μm, 40 μm, and 60 μm, respectively. It is worth noting that the smaller the waist diameter, the smaller the FSR. In the characterization and measurement steps, each spectrum was processed using a peak fitting function to identify the value

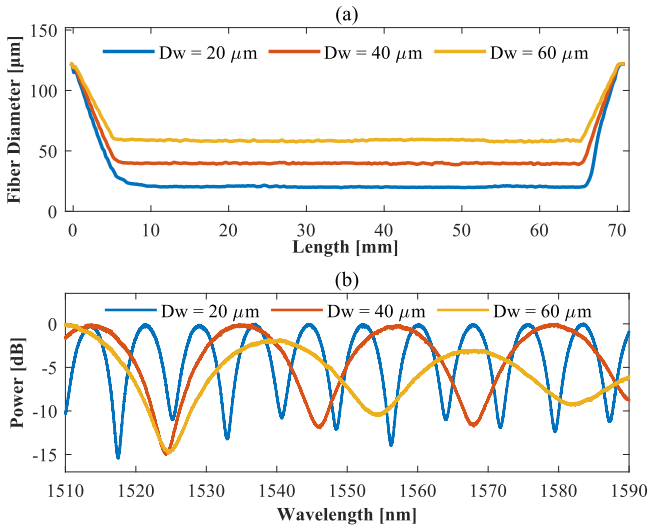

Fig. 2. (a) MCF taper diameter measurements. (b) Normalized transmission spectra of the central core.

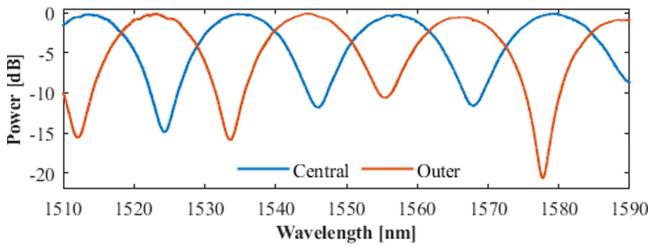

Fig. 3. Transfer function of the central and outer core of the MCF taper with a waist diameter of 40 μm.

of the wavelength dips. The measurement resolution is limited by the equipment resolution and the full width at half maximum (FWHM) of the dips [18]. The FWHM values are 1.29 nm, 3.76 nm, and 4.41 nm for waist diameters of 20 μm, 40 μm, and 60 μm, respectively. Accordingly, a resolution of 5 pm belonging to the detection equipment represents 0.38%, 0.13%, and 0.11% of the FWHM of the evaluated waist diameters, in increasing order.

The multiplexing devices allow us to measure the coupled transmitted power in the outer cores when the light is injected into the central core. Fig. 3 shows the transfer function of the central and one outer core of the MCF coupler with a waist diameter of 40 μm. It is observed that the transfer function of the outer core is approximately $\frac{\pi}{2}$ shifted compared to that of the central core, as described by (2) and (3).

The sensors were measured using an interrogation module with an accuracy of 1 pm (SM125, Micron Optic), as depicted in Fig. 4, which operates within a wavelength range from 1510 nm to 1590 nm. The light was injected from channel one (top channel in the figure) of the interrogator, while the transmitted signal from the sensor was received in the second channel. Since interrogation modules inject light and measure the reflected signal, an isolator was essential to suppress the injected light

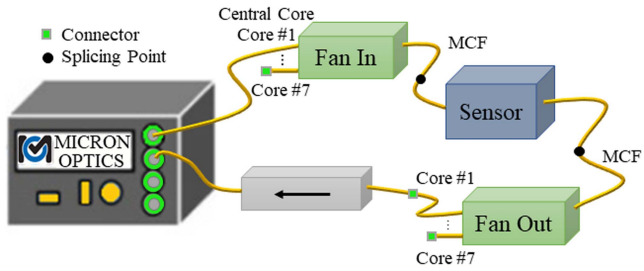

Fig. 4. Central core interrogation setup.

from the receiving channel, and therefore, enable the reception of the signal.

III. Temperature and Strain Measurements

A. Temperature

The sensors were placed into a high-temperature tube furnace to investigate the temperature sensitivity. The optical fiber was carefully positioned in the furnace between two translation stages, which also subjected the fiber to a small amount of strain to prevent any sagging of the fiber due to gravity in the furnace. The temperature was set from 100 °C to 600 °C with steps of 25 °C. The stabilization process of the furnace took about 30 minutes at every step. The light was injected into the central core, and the outputs from the central and outer cores were monitored by the interrogator.

The transmitted optical signals of the central core of each of our three sensors, at different temperatures, are shown in Fig. 5. All sensors show a red shift with temperature increments. A wavelength dip around 1550 nm was selected for each measured transmission spectrum, using a peak fitting function, in order to analyze the wavelength shift and study the effect of the waist diameter on the temperature sensitivity. Fig. 5(a), (b) and (c) show the wavelength dips of the sensors with waist diameters of 20 μm, 40 μm, and 60 μm, revealing a total wavelength shift of approximately 10 nm, 16 nm, and 30 nm, respectively.

The wavelength shifts of the three sensors as a function of the temperature are illustrated in Fig. 6. The fitted equation for each curve, displayed in the figure, is a quadratic function with a coefficient of determination, R^2, above 0.99. If the temperature measurement data from 225 °C to 600°C are linearly fitted with a coefficient of determination $R^2 = 0.99$, as shown by the red dashed lines in Fig. 6, temperature sensitivities of approximately 19.6 pm/°C, 35.4 pm/°C, and 62.1 pm/°C in the central core are obtained for waist diameters of 20 μm, 40 μm, and 60 μm, respectively. As observed, the sensor with a larger waist diameter has a larger wavelength shift, leading to a better sensitivity. Moreover, according to the FSR value of each sensor (see Fig. 2(b)), unequivocal high-temperature measurements span over a range of around 390 °C, 620 °C, and 470 °C, for the evaluated waist diameters, in increasing order.

The quadratic trend of the wavelength shift could be attributed to the nonlinear relationship between the temperature and the refractive index of silica fiber for high-temperature ranges [19],

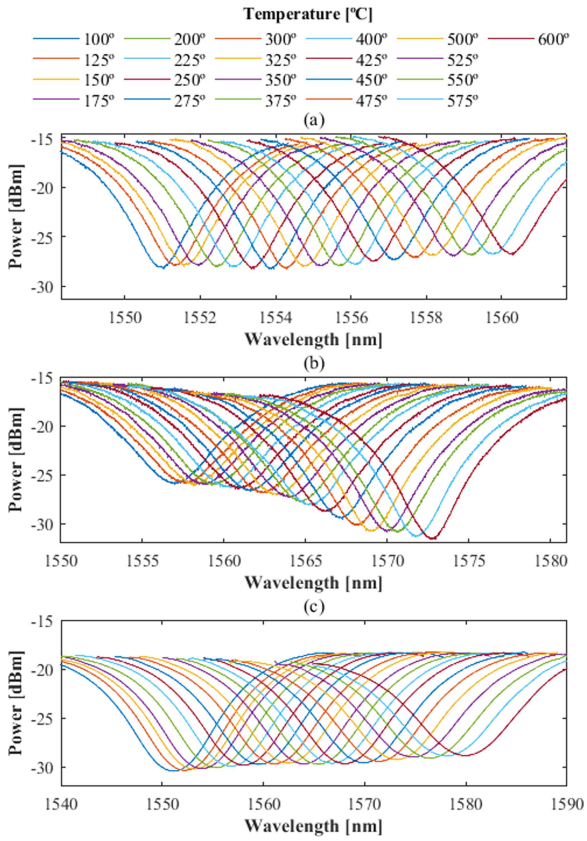

Fig. 5. Transmission spectra of the central core showing a red shift with increasing temperature, for sensors with waist diameters of (a) Dw = 20 μm, (b) Dw = 40 μm, and (c) Dw = 60 μm.

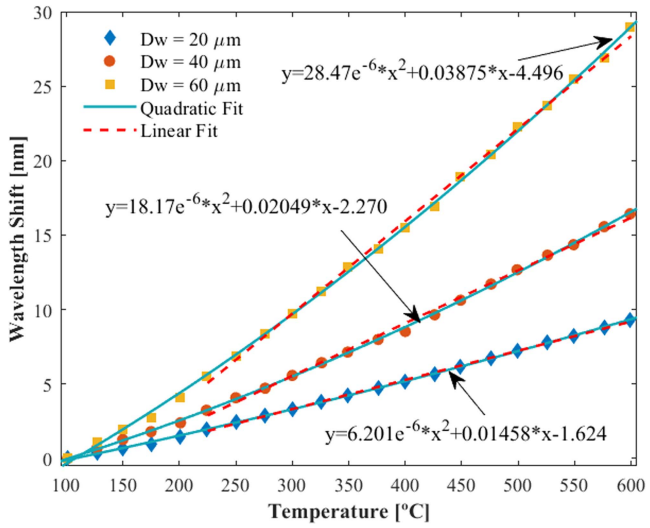

Fig. 6. Wavelength shifts of the central core at different temperatures.

expressed as

$$n\ (T) = \ n_0 + \alpha_n T + \beta_n T^2, \tag{4}$$

where α_n and β_n are the first and second orders of the thermo-optic coefficient. Based on this relationship, the wavelength shift, and consequently the sensitivity, can also be reasonably

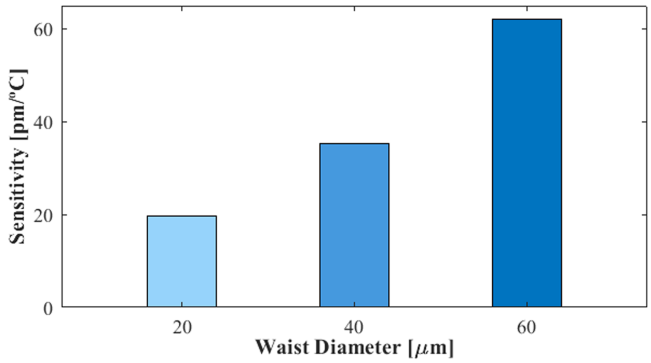

Fig. 7. Temperature sensitivity variation as a function of the taper waist diameter.

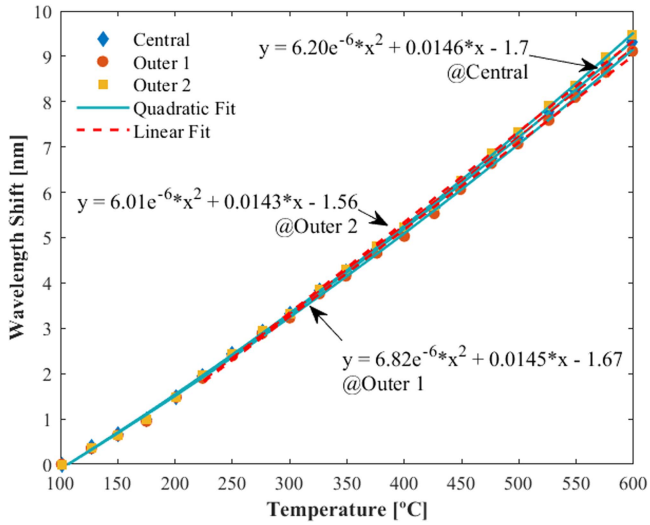

Fig. 8. Wavelength shift of the central and outer cores of the 20 μm waist diameter MCF taper at different temperatures.

assumed to depend quadratically on temperature. The dependence of the temperature sensitivity values on the waist diameter of the MCF taper is presented in Fig. 7. While the results suggest that the sensitivity has a nonlinear dependency on the waist diameter, additional data at other waist diameters are needed to mathematically verify this hypothesis.

The data collected from two of the outer cores of the MCF coupler with a waist diameter of 20 μm are shown in Fig. 8. It is noted that these curves also correspond to a quadratic function. Applying a linear fit, represented by red dashed lines with R^2-values above 0.9, to the data from 225 °C to 600 °C gives a temperature sensitivity of approximately 19.1 pm/°C and 19.9 pm/°C in outer cores 1 and 2, respectively. It is observed that the outer cores have a temperature sensitivity different from that of the central core. This could be attributed to slight differences in their initial refractive indices inherent in the MCF. Moreover, it would be expected that if there were differences in sensitivity between the outer cores and the central core, they would be symmetrical since the cores of the optical fiber are equidistantly distributed. However, outer core 1 has a sensitivity value lower

TABLE I
SENSITIVITY VALUES FOR TEMPERATURE VARIATIONS FROM 225 TO 600 °C

Waist Diameter [μm]	R^2	Temperature Sensitivity [pm/ºC]		
		Central	Outer 1	Outer 2
20	0.999	19.6	19.1	19.9
40	0.996	35.4	32.3	35.3
60	0.998	62.1	57.6	60.1

than the others. Since the two selected outer cores are opposites, this could mean that a slight bending has occurred as a result of the optical fiber being suspended in the air inside the tube furnace. Thus, we should consider that the refractive index of the core could also be affected by bending, represented by [20]

$$n_b = n_o\left[1 + (r\kappa)\cos\left(\phi\right)\right], \tag{5}$$

where n_b is the refractive index of the bended core, n_o is the refractive index of the core in the straight fiber, and $\kappa = \frac{1}{R}$ is the curvature, with R being the bending radius. The parameters r and ϕ are the polar coordinates. Variations in the refractive index of the cores lead to changes in the coupling coefficients among them, which consequently affect the sensitivity of the temperature sensors. Hence, the temperature sensitivity of each core in this experiment could depend on the refractive index variations in the core caused by the temperature changes and slight bending of the MCF. To verify this complex scenario, it would be essential to simulate the response of the sensor taking into account several details, such as the fact that the thermal expansion coefficient inherent in the optical fiber could cause the stripped optical fiber length inside the tube to expand. Without precise strain control, this expansion could cause the fiber to deviate from a straight line and potentially lead to buckling or bending [21], [22]. Additionally, the linear fitting might vary based on the chosen temperature range, and torsion could also be a factor to consider.

Table I shows the temperature sensitivity values of the central and outer cores of the three sensors. It should be noted that the difference between the outer cores has the same trend. In all cases, the temperature sensitivity of outer core 2 is higher than that of outer core 1. However, for waist diameters of 40 μm and 60 μm, although the temperature sensitivity of outer core 2 is greater than that of outer core 1, it is lower than that of the central core. This could be due to the lower coupling coefficient associated with larger taper waist diameters [4].

All in all, our measurements show that for increasing the sensitivity of a tapered-MCF temperature sensor, one should avoid large coupling coefficients among the cores, which means that the taper waist diameter should not be very small. Furthermore, we do not observe a considerable difference between the sensitivity of the central core and that of the outer cores, indicating that it is sufficient to only monitor the central core in the proposed MCF-based temperature sensors.

In addition to the peak fitting method described earlier, various other techniques can be employed to analyze the response of the sensors. These include frequency domain analysis, cross-correlation, and subpixel resolution methods. We compared the

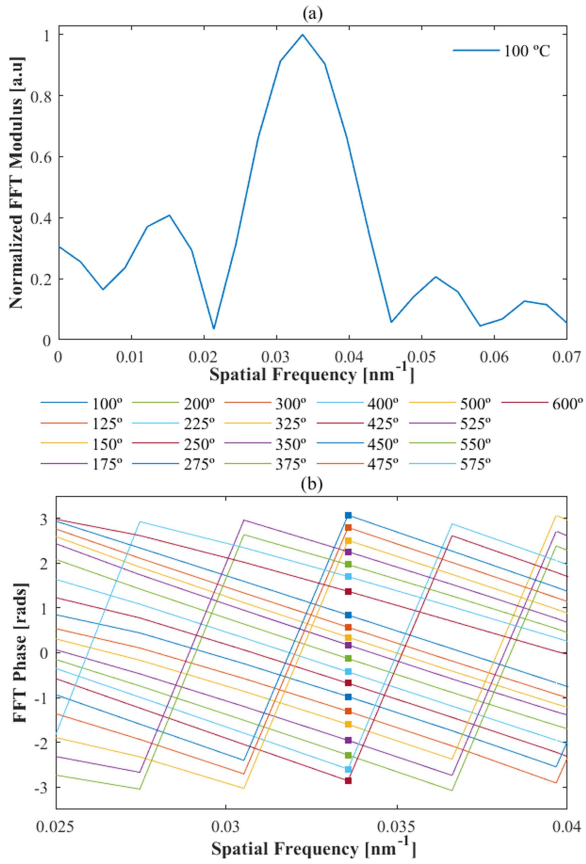

Fig. 9. Frequency domain analysis: (a) Normalized FFT modulus. (b) FFT phase of each high-temperature measurement response.

results obtained from three different methods to assess the robustness and accuracy of our sensor calibration across different analytical methodologies. Specifically, we applied frequency domain analysis and cross-correlation techniques to derive the total wavelength shift for each scenario. Subsequently, we compared these results with those obtained through the peak fitting function. For this analysis, we utilized the optical spectrum responses of the tapered MCF with a waist diameter of 60 μm.

The modulus and phase obtained from the applied Fast Fourier Transform (FFT) in the frequency domain analysis are illustrated in Fig. 9. The FFT modulus of the sensor response at 100 °C is depicted in Fig. 9(a). A similar response is obtained at other measured temperatures. They all consistently reveal a peak at a spatial frequency of 0.336. This value is a crucial indicator for selecting the corresponding phase value for each high-temperature measurement response, as demonstrated in Fig. 9(b). Considering each phase value, we can determine the total wavelength shift [23], using

$$\Delta\,\lambda_i = \frac{\Delta\theta_i}{2\pi v_i}, \tag{6}$$

where v_i is the corresponding spatial frequency for each phase θ_i. The determined total wavelength shifts found through frequency domain analysis are shown in Fig. 11.

The cross-correlation analysis for the measured high-temperature responses, to determine the wavelength shift, is

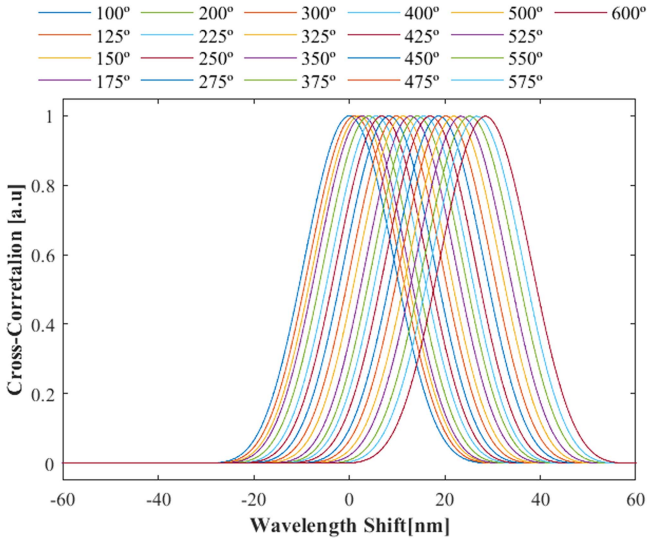

Fig. 10. Cross-correlation analysis of the measured high-temperature responses.

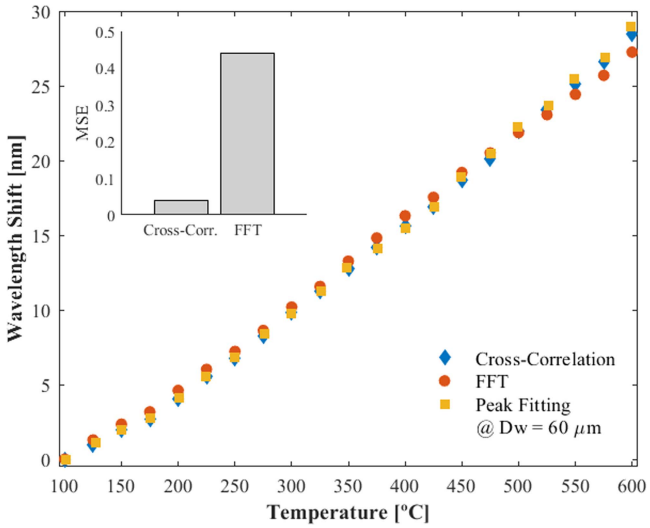

Fig. 11. Comparison of wavelength shift analysis methods: Cross-correlation, FFT, and peak fitting.

presented in Fig. 10. The resolution value utilized in the algorithm aligns with the interrogator module resolution for precise analysis. Cross-correlation identifies the shift in each optical spectrum compared to its predecessor. It should be noted that the peak value of each correlation graph represents the wavelength shift of each measurement. The total wavelength shift obtained by cross-correlation analysis is shown in Fig. 11.

After studying the three proposed methods, the determined total wavelength shift for each one is depicted in Fig. 11. It is observed that the results from the peak fitting and cross-correlation methods exhibit similarity, contrasting with the findings from the frequency domain analysis, which diverges from those of the peak fitting method. We calculated the mean squared error (MSE) for both frequency domain analysis and cross-correlation compared to the peak fitting method to quantify the accuracy of

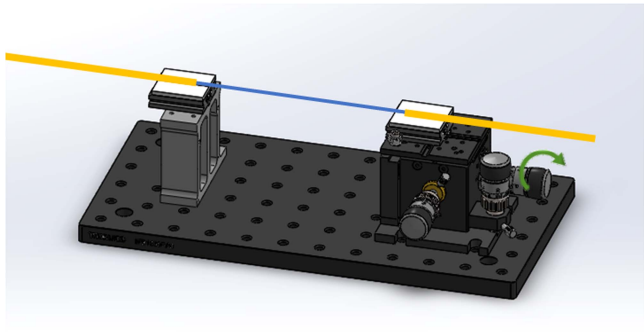

Fig. 12. Strain measurement setup.

each one. The cross-correlation method demonstrates a notably lower MSE. This indicates that the peak fitting and cross-correlation methods offer superior analytical precision for the selected MCF taper. Conversely, the frequency domain analysis method yields a larger MSE. This could be attributed to the FFT requiring more optical spectrum periods to accurately determine the spatial frequencies and their corresponding phase values. This makes this method less optimal for analyzing tapered MCF sensors with large periods.

B. Strain

The sensors were fixed using standard V-groove fiber holders for strain sensitivity measurements. One of the holders was placed on top of a translation stage, while the other was mounted on a fixed stage, as shown in Fig. 12. The distance separation between the holders was set to 18 cm, and the translation stage was moved in steps of 50.0 μm. The strain setting changed from 0.0 $\mu\varepsilon$ up to 3333.33 $\mu\varepsilon$.

The dependence of the transmitted signal in the central core on strain variations is shown in Fig. 13 for the three different sensors, where it can be clearly seen that increasing the strain leads to a shift of the spectra. The spectral dip nearest to 1550 nm was selected from each sensor to analyze the waist diameter effect on the strain sensitivity. As depicted in Fig. 13(a), (b), and (c), the sensors with waist diameters of 20 μm, 40 μm, and 60 μm exhibit total wavelength shifts of around 18 nm, 12 nm, and 6 nm, respectively. Fig. 14 shows the total wavelength shift of the three sensors. It can be observed that the sensor with a smaller waist diameter has a higher wavelength shift. The negative sign observed in the wavelength shift, indicates that the optical spectra are shifted towards shorter wavelengths (blue-shift). To determine the sensitivity, all monitored wavelength shifts were linearly fitted with an R^2 value above 0.99. Strain sensitivities of -5.2 pm/$\mu\varepsilon$, -3.3 pm/$\mu\varepsilon$, and -1.5 pm/$\mu\varepsilon$ are reported for waist diameters of 20 μm, 40 μm, and 60 μm, respectively. It is important to note that besides the taper waist diameter, the waist length and the gauge length affect the strain sensitivity [15]. Thus, the sensitivities reported here may vary depending on the waist length and gauge length. The strain gauge of the sensing head of our proposed sensor is the taper length, $L_{taper} = 2L_t + L_w$. Considering the FSR values obtained from

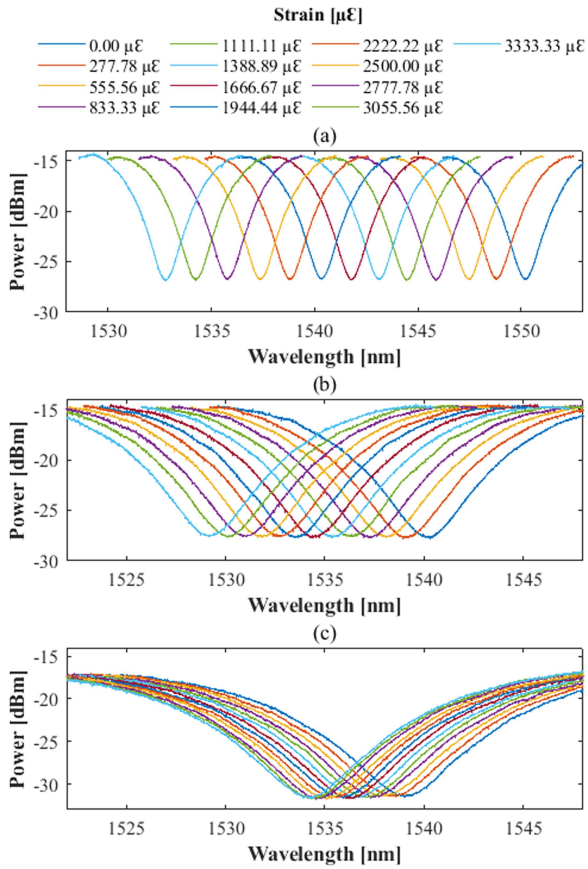

Fig. 13. Transmission spectra of the central core showing a blue-shift with increasing strain, for sensors with waist diameters of (a) Dw = 20 μm, (b) Dw = 40 μm, and (c) Dw = 60 μm.

Fig. 2(b), the range of strain for unequivocal measurements is around 1486 $\mu\varepsilon$, 6651 $\mu\varepsilon$, and 19680 $\mu\varepsilon$ for waist diameters of 20 μm, 40 μm, and 60 μm, respectively.

Due to the elasto-optic effect, the effective refractive index in silica fiber (n_{eff}) varies when subjected to strain. This variation has a linear relationship with the elastic-optical coefficient [24], given by

$$\Delta n_{eff} = \gamma n \varepsilon, \tag{7}$$

where n is the unperturbed refractive index, and γ and ε are the elasto-optic coefficient and axial strain, respectively. To analyze the strain sensitivity trend based on the waist diameter, we have plotted the strain sensitivity values against the waist diameter for each sensor, as depicted in Fig. 15. We can observe that the strain sensitivity increases as the waist diameter decreases. To mathematically model the relationship between the strain sensitivity and the waist diameter, additional data from other sensors with different waist diameters is required.

The comparison of the wavelength shift response between the central and two outer cores of the sensor with a waist diameter of 20 μm is displayed in Fig. 16. The three graphs have the same slope. Table II shows that the strain sensitivity values of the central and outer cores of the three sensors are the same. This represents the symmetry of the fabricated taper region. Given that our measurements show identical sensitivity

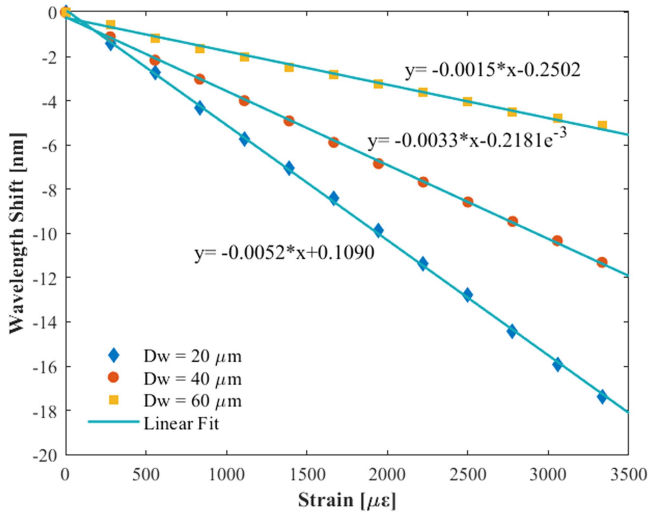

Fig. 14. Wavelength shifts of the central core at different strains, at room temperature.

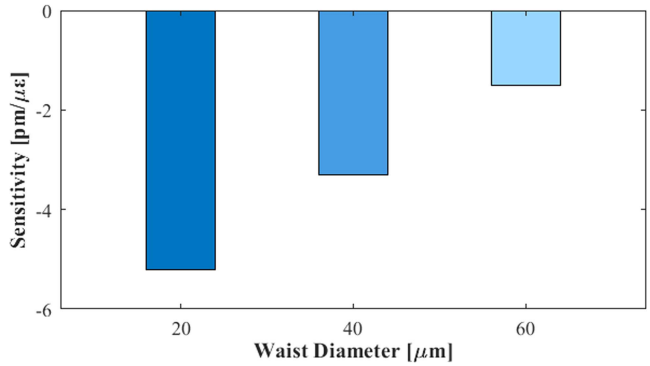

Fig. 15. Strain sensitivity variation as a function of the taper waist diameter. The negative sign shows that the optical spectra shift towards shorter wavelengths as the strain increases.

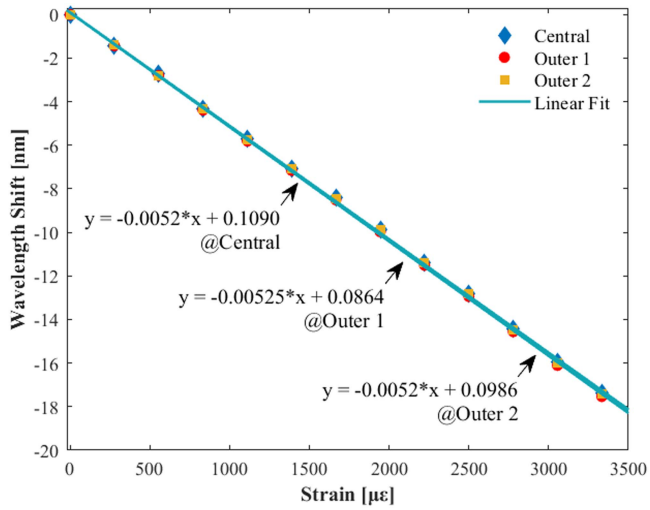

Fig. 16. Wavelength shift of the central and outer cores of the 20 μm waist diameter MCF taper at different strains, at room temperature.

TABLE II
SENSITIVITY VALUES FOR STRAIN VARIATIONS

Waist Diameter [μm]	R^2	Strain Sensitivity [pm/με]		
		Central	Outer 1	Outer 2
20	0.999	-5.2	-5.25	-5.2
40	0.999	-3.3	-3.3	-3.3
60	0.995	-1.5	-1.5	-1.5

for the central and outer cores, it suffices to only monitor the central core in strain sensors fabricated in this type of fiber. At this point, we have determined the sensitivity of our high-temperature and strain sensors. Our observations show that the core sensitivities are only slightly different for the two evaluated parameters. Consequently, determining a cross-sensitivity matrix would not effectively compensate for simultaneous temperature and strain measurements. To solve this issue and manage the cross-sensitivity, we propose combining two tapered multicore sensors.

IV. CONCLUSION

We have analyzed the effect of the waist diameter on the sensitivity of strain and temperature sensors based on tapered multicore structures. Three sensors were fabricated with a non-adiabatic tapering technique. All sensors have a waist length of 60 mm but feature different waist diameters of 20 μm, 40 μm, and 60 μm, respectively. These sensors demonstrated sensitivities of approximately 19.6 pm/°C, 35.4 pm/°C, and 62.1 pm/°C, respectively, for temperature variations within the range of 225 °C to 600 °C. Meanwhile, for strain variations ranging from 0.0 $\mu\varepsilon$ to 3333.33 $\mu\varepsilon$, we obtained sensitivities of -5.2 pm/$\mu\varepsilon$, -3.3 pm/$\mu\varepsilon$ and -1.5 pm/$\mu\varepsilon$ for the three sensors, respectively. It is noteworthy that a smaller waist diameter shows the best sensitivity for strain measurements, while in contrast, the taper with 60 μm of waist diameter is better for temperature measurements. These findings could significantly contribute to the optimal design of tapered multicore sensors and provide valuable insights for researchers interested in this area.

ACKNOWLEDGMENT

Author Valeria Hernández-Ambato would like to extend her deepest gratitude to her late mother, Ms. Martha Ambato Collaguazo, for her valuable support and encouragement throughout the course of this research. The authors would also like to thank the anonymous reviewers for their insightful comments, which have greatly improved the quality of this manuscript.

REFERENCES

[1] J. E. Antonio-Lopez, Z. S. Eznaveh, P. LiKamWa, A. Schülzgen, and R. Amezcua-Correa, "Multicore fiber sensor for high-temperature applications up to 1000°C," *Opt. Lett.*, vol. 39, no. 15, pp. 4309–4312, Aug. 2014, doi: 10.1364/ol.39.004309.

[2] A. Miliou, "In-fiber interferometric-based sensors: Overview and recent advances," *Photonics*, vol. 8, no. 7, Jul. 2021, Art. no. 265, doi: 10.3390/photonics8070265.

[3] J. Tian, Y. Jiao, S. Ji, X. Dong, and Y. Yao, "Cascaded-cavity Fabry–Perot interferometer for simultaneous measurement of temperature and strain with cross-sensitivity compensation," *Opt. Commun.*, vol. 412, pp. 121–126, Apr. 2018, doi: 10.1016/j.optcom.2017.12.005.

[4] Y. Chunxia, D. Hui, D. Wei, and X. Chaowei, "Weakly-coupled multicore optical fiber taper-based high-temperature sensor," *Sensors Actuators A: Phys.*, vol. 280, pp. 139–144, Sep. 2018, doi: 10.1016/j.sna.2018.07.016.

[5] M. Pandey and G. Mishra, "Types of sensor and their applications, advantages, and disadvantages," *Emerg. Technol. Data Mining Inf. Secur.*, vol. 814, pp. 791–804, 2019, doi: 10.1007/978-981-13-1501-5_69.

[6] X. Jiang, K. Kim, S. Zhang, J. Johnson, and G. Salazar, "High-temperature piezoelectric sensing," *Sensors*, vol. 14, no. 1, pp. 144–169, Jan. 2014, doi: 10.3390/s140100144.

[7] F. Mumtaz, Y. Dai, and M. A. Ashraf, "Inter-cross de-modulated refractive index and temperature sensor by an etched multi-core fiber of a MZI structure," *J. Lightw. Technol.*, vol. 38, no. 24, pp. 6948–6953, Dec. 2020, doi: 10.1109/JLT.2020.3014857.

[8] A. Van Newkirk, J. E. Antonio-Lopez, G. Salceda-Delgado, M. U. Piracha, R. Amezcua-Correa, and A. Schülzgen, "Multicore fiber sensors for simultaneous measurement of force and temperature," *IEEE Photon. Technol. Lett.*, vol. 27, no. 14, pp. 1523–1526, Jul. 2015, doi: 10.1109/LPT.2015.2427733.

[9] D. Barrera, J. Madrigal, and S. Sales, "Tilted fiber Bragg gratings in multicore optical fibers for optical sensing," *Opt. Lett.*, vol. 42, no. 7, pp. 1460–1463, Apr. 2017, doi: 10.1364/ol.42.001460.

[10] L. Gan et al., "Spatial-division multiplexed Mach-Zehnder interferometers in heterogeneous multicore fiber for multiparameter measurement," *IEEE Photon. J.*, vol. 8, no. 1, Feb. 2016, Art. no. 7800908, doi: 10.1109/JPHOT.2016.2516254.

[11] Y. Yao, Z. Zhao, and M. Tang, "Advances in multicore fiber interferometric sensors," *Sensors*, vol. 23, no. 7, Apr. 2023, Art. no. 3436, doi: 10.3390/s23073436.

[12] H. Zhang et al., "Highly sensitive strain sensor based on helical structure combined with Mach-Zehnder interferometer in multicore fiber," *Sci. Rep.*, vol. 7, Apr. 2017, Art. no. 46633, doi: 10.1038/srep46633.

[13] D. Guo et al., "Tapered multicore fiber interferometer for refractive index sensing with graphene enhancement," *Appl. Opt.*, vol. 59, no. 13, May 2020, Art. no. 3927, doi: 10.1364/ao.385324.

[14] Z. Tang, S. Lou, X. Wang, B. Huang, M. Wang, and X. Sheng, "Sensitivity optimization of symmetric multi-core fiber strain sensor based on mode-coupling theory," *Infrared Phys. Technol.*, vol. 111, Dec. 2020, Art. no. 103517, doi: 10.1016/j.infrared.2020.103517.

[15] O. Frazão, S. F. O. Silva, A. Guerreiro, J. L. Santos, L. A. Ferreira, and F. M. Araújo, "Strain sensitivity control of fiber Bragg grating structures with fused tapers," *Appl. Opt.*, vol. 46, no. 36, pp. 8578–8582, Dec. 2007, doi: 10.1364/AO.46.008578.

[16] A. W. Snyder, "Coupled-mode theory for optical fibers," *J. Opt. Soc. Amer.*, vol. 62, no. 11, pp. 1267–1277, Nov. 1972, doi: 10.1364/JOSA.62.001267.

[17] M.-S. Yoon, S.-B. Lee, and Y.-G. Han, "In-line interferometer based on intermodal coupling of a multicore fiber," *Opt. Exp.*, vol. 23, no. 14, pp. 18316–18322, Jul. 2015, doi: 10.1364/oe.23.018316.

[18] I. M. White and X. Fan, "On the performance quantification of resonant refractive index sensors," *Opt. Exp.*, vol. 16, no. 2, pp. 1020–1028, Jan. 2008, doi: 10.1364/OE.16.001020.

[19] H. Gao, Y. Jiang, Y. Cui, L. Zhang, J. Jia, and L. Jiang, "Investigation on the thermo-optic coefficient of silica fiber within a wide temperature range," *J. Lightw. Technol.*, vol. 36, no. 24, pp. 5881–5886, Dec. 2018, doi: 10.1109/JLT.2018.2875941.

[20] D. Pallares-Aldeiturriaga, L. Rodriguez-Cobo, A. Quintela, and J. M. Lopez-Higuera, "Curvature sensor based on in-fiber Mach-Zehnder interferometer inscribed with femtosecond laser," *J. Lightw. Technol.*, vol. 35, no. 21, pp. 4624–4628, Nov. 2017, doi: 10.1109/JLT.2017.2756103.

[21] D. Barrera, J. Hervás, I. Gasulla, and S. Sales, "Enhanced accuracy sensors using multicore optical fibres based on RFBGs for temperatures up to 1000°C," in *Proc. 6th Eur. Workshop Opt. Fibre Sensors*, May. 2016, pp. 99161J1–99161J4, doi: 10.1117/12.2236617.

[22] T. S. Priest, K. T. Jones, G. B. Scelsi, and G. A. Woolsey, "Thermal coefficients of refractive index and expansion in optical fibre sensing," presented at the 12th Int. Conf. Opt. Fiber Sensors, Williamsburg, VA, USA, 1997, Paper OWC41, doi: 10.1364/OFS.1997.OWC41.

[23] D. Barrera et al., "Low-loss photonic crystal fiber interferometers for sensor networks," *J. Lightw. Technol.*, vol. 28, no. 24, pp. 3542–3547, Dec. 2010, doi: 10.1109/JLT.2010.2090861.

[24] C. Zhang et al., "An optical fiber strain sensor by using of taper based TCF structure," *Opt. Laser Technol.*, vol. 120, Dec. 2019, Art. no. 105687, doi: 10.1016/j.optlastec.2019.105687.